

Minority-spin conduction in ferromagnetic $\text{Mn}_5\text{Ge}_3\text{C}_x$ and $\text{Mn}_5\text{Si}_3\text{C}_x$ films derived from anisotropic magnetoresistance and density functional theory

Sihao Deng^{1,2}, Rolf Heid³, Klaus-Peter Bohnen³, Cong Wang⁴, and Christoph Sürgers¹

¹Physikalisches Institut, Karlsruhe Institute of Technology, Wolfgang Gaede Straße 1, 76131 Karlsruhe, Germany

²Spallation Neutron Source Science Center, 523803 Dongguan, People's Republic of China

³Institute for Quantum Materials and Technologies, Karlsruhe Institute of Technology, Hermann-von-Helmholtz-Platz 1, 76344 Eggenstein-Leopoldshafen, Germany

⁴School of Integrated Circuit Science and Engineering, Beihang University, 37 Xueyuan Rd, 100191 Beijing, People's Republic of China



(Received 1 February 2021; revised 12 April 2021; accepted 13 April 2021; published 27 April 2021)

The anisotropic magnetoresistance (AMR) of ferromagnetic $\text{Mn}_5\text{Ge}_3\text{C}_x$ ($0 \leq x \leq 1$) and $\text{Mn}_5\text{Si}_3\text{C}_x$ ($0.5 \leq x \leq 1$) thin films was investigated and compared with density functional theory calculations from which the spin-split electronic density of states at the Fermi level and the spin polarization were obtained. The isostructural compounds exhibit different AMR behavior. While only $\text{Mn}_5\text{Si}_3\text{C}_{0.5}$ shows a positive AMR ratio and a positive spin polarization, the negative AMR ratio of all other compounds is due to a negative spin polarization. The correlation between the sign of the AMR and the degree of spin polarization is in agreement with theoretical calculations of the AMR ratio indicating that the magnetoelectronic transport in both compounds is dominated by minority-spin conduction. The dominating role of minority-spin conduction remains unaffected even after incorporation of carbon into the crystalline lattice which weakens both AMR and spin polarization.

DOI: [10.1103/PhysRevB.103.134439](https://doi.org/10.1103/PhysRevB.103.134439)

I. INTRODUCTION

Magnetic materials for spin injection and manipulation into semiconductor heterostructures are important for the realization of future spintronic applications and devices [1,2]. In general, metallic ferromagnets on semiconductors bear the disadvantage of a conductivity mismatch thus preventing an efficient spin injection from the metal into the semiconductor. In search of suited materials for spin injection into semiconducting Ge, the intermetallic compound Mn_5Ge_3 has been proposed as a promising candidate due to its high resistivity and compatibility with complementary metal-oxide-semiconductor (CMOS) technology [3–5]. First experiments demonstrating spin injection from Mn_5Ge_3 into Si or Ge have been reported [6,7]. Mn_5Ge_3 is also an interesting material for the development of novel spintronic devices in combination with graphene [8]. However, the Curie temperature T_C of Mn_5Ge_3 is about room temperature, which is quite low for usual applications. A promising way to enhance the ferromagnetic stability is to incorporate carbon into the lattice, thereby boosting T_C to 450 K for $\text{Mn}_5\text{Ge}_3\text{C}_{0.8}$ [4,9].

The isostructural but antiferromagnetic Mn_5Si_3 can be similarly modified by the incorporation of carbon to show an enhanced ferromagnetic stability up to $T_C = 350$ K for $\text{Mn}_5\text{Si}_3\text{C}_{0.8}$ [10]. While ferromagnetic $\text{Mn}_5\text{Ge}_3\text{C}_{0.8}$ and $\text{Mn}_5\text{Si}_3\text{C}_{0.8}$ exhibit similar properties with regard to their crystalline structure and magnetic ordering, a previous magnetotransport study has shown that the anisotropic magnetoresistance (AMR) in these compounds shows a different behavior.

The AMR is due to spin-orbit scattering and the AMR ratio is usually expressed as $\Delta\rho/\rho = (\rho_{\parallel} - \rho_{\perp})/\rho_{\perp}$, where ρ_{\parallel} and ρ_{\perp} are the zero-field extrapolated magnetoresistivities when the magnetization is applied parallel or perpendicularly to the current direction, respectively [11]. In most metallic ferromagnets the AMR is positive while a negative AMR has been taken as an indication for minority-spin conduction as seen in, e.g., in iron nitride films [12]. For iron nitride films, an extended theory for the AMR based on the two-current model proposed earlier by Mott and Campbell and Fert was developed [13,14]. It takes into account the different scattering channels and allows to correlate the size of the AMR ratio with the degree of spin polarization $P_0 = (N_{\uparrow} - N_{\downarrow})/(N_{\uparrow} + N_{\downarrow})$, where $N_{\uparrow(\downarrow)}$ is the electronic density of states (DOS) at the Fermi level E_F of electrons in the majority (N_{\uparrow}) and minority (N_{\downarrow}) spin subbands, respectively [15]. N_{\uparrow} and N_{\downarrow} can be obtained from first principle calculations using density functional theory (DFT) and directly enter into the modified expression for the AMR ratio. P_0 can be experimentally obtained from spin-resolved photoemission spectroscopy [16].

Although DFT was used earlier to study the electronic band structure and magnetic properties of Mn_5Ge_3 and $\text{Mn}_5\text{Ge}_3\text{C}_{0.8}$ [17–22], an investigation of the concentration dependence of AMR and DFT has not been done so far. In addition, DFT calculations are so far not available for isostructural ferromagnetic $\text{Mn}_5\text{Si}_3\text{C}_x$. In this work we report a combined investigation of the spin polarization P_0 and the AMR ratio of $\text{Mn}_5\text{Ge}_3\text{C}_x$ ($0 \leq x \leq 1$) and $\text{Mn}_5\text{Si}_3\text{C}_x$ ($0.5 \leq x \leq 1$) films revealing a minority-spin conduction in both compounds and a decreasing spin polarization P_0 with increasing carbon content x . We stress that we only consider P_0 which directly enters

into the theoretical model for the AMR ratio [13,14] and not the spin polarization of the electric current for which the spin-dependent Fermi velocities averaged over the Fermi surface have to be taken into account [15].

II. EXPERIMENT

Fifty-nm thick films were deposited onto (1120)-oriented sapphire substrates by magnetron sputtering from independent elemental targets in Ar atmosphere as described earlier [9,10,23]. The nominal Mn, Ge, Si, and C concentrations were calculated from calibrated sputtering rates of the individual targets.

The films were structurally characterized by x-ray diffraction using Cu K_α radiation. We only mention that films sputtered on Ge(111) substrates did show an epitaxial in-plane relation between Ge(111) and $\text{Mn}_5\text{Ge}_3\text{C}_x(0002)$. This was confirmed by ϕ scans around the (1123) reflection showing well-resolved peaks separated by 60° due to the six-fold symmetry of the hexagonal crystallographic lattice of the films. The six-fold symmetry in the (0002) plane gives rise to an in-plane hexagonal anisotropy with one easy axis along the [100] direction of the film as reported for high-quality epitaxially grown films on Ge(111) [24].

In contrast, the present sputtered films deposited on sapphire did show a random orientation of the crystallographic grains in the film plane as inferred from missing peaks in the ϕ scans. However, some preferential growth perpendicular to the film plane, in particular along the hexagonal c axis, was observed [25].

Electronic transport measurements were done on Hall bar structures obtained by depositing the film through a mechanical mask. The magnetoresistance was measured as a function of temperature T and magnetic field H applied either parallel or perpendicularly to the current direction. Field and current were applied in the film plane, see inset Fig. 3(b).

DFT calculations were performed for $\text{Mn}_5\text{Ge}_3\text{C}_x$ and $\text{Mn}_5\text{Si}_3\text{C}_x$ for various x using the projector-augmented wave (PAW) method initially proposed by Blöchl [26,27]. We used the execution of Kresse and Joubert in the Vienna *ab initio* Simulation Package (VASP) code [28–31] within the generalized gradient approximation (GGA) [32,33] to calculate the fully unconstrained magnetic structures. The cutoff energy of the plane wave was assumed to be 500 eV. The Monkhorst-Pack k -point sampling was adopted, corresponding to $2 \times 4 \times 5$ for $x = 0.75$ and $4 \times 4 \times 6$ for all other compounds. We used supercells comprising two or four formula units, i.e., $\text{Mn}_{10}\text{Ge}_6$, $\text{Mn}_{10}\text{Ge}_6\text{C}$, $\text{Mn}_{20}\text{Ge}_{12}\text{C}_3$, and $\text{Mn}_{10}\text{Ge}_6\text{C}_2$ for our calculations corresponding to $\text{Mn}_5\text{Ge}_3\text{C}_x$ with $x = 0, 0.5, 0.75$, and 1, respectively. For Mn_5Si_3 which orders antiferromagnetically below $T = 100$ K we could not obtain reasonable results by DFT and therefore considered only $\text{Mn}_5\text{Si}_3\text{C}_x$ for $x = 0.5, 0.75$, and 1.

III. RESULTS

A. DFT calculations

The hexagonal unit cell comprising two formula units of $\text{Mn}_5\text{Ge}_3\text{C}$ with Mn_5Si_3 -type structure (space group $P6_3/mcm$) is shown in Fig. 1(a). The two inequivalent Mn

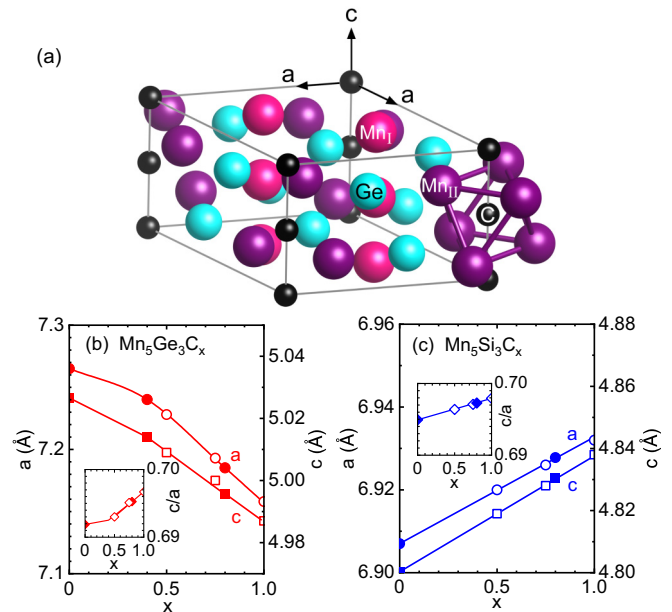


FIG. 1. (a) Hexagonal unit cell of $\text{Mn}_5\text{Ge}_3\text{C}$. The two inequivalent Mn sites are labeled Mn_I and Mn_{II} . One Mn_{II} octahedra surrounding C at the $2(b)$ position is shown, see text for details. The image was created by using the VESTA code [37]. (b) Lattice parameters a and c of the hexagonal unit cell of 50-nm-thick $\text{Mn}_5\text{Ge}_3\text{C}_x$ films determined by x-ray diffraction (solid symbols), see Ref. [25]. Open symbols indicate values obtained from a linear interpolation between measured values which have been used as input parameters for the DFT calculations. Inset shows the c/a ratio. (c) Lattice parameters of $\text{Mn}_5\text{Si}_3\text{C}_x$ films.

sites are labeled Mn_I and Mn_{II} . Previous reports assumed that carbon occupies the $2(b)$ voids formed by Mn_{II} octahedra at the $6(g)$ lattice sites [9,34]. This has been nicely confirmed by a recent ^{55}Mn nuclear magnetic resonance (NMR) investigation performed on an epitaxially grown $\text{Mn}_5\text{Ge}_3\text{C}_{0.2}$ film on Ge(111) [35].

DFT calculations for Mn_5Ge_3 and $\text{Mn}_5\text{Ge}_3\text{C}_{0.8}$ have been published earlier [17–22]. DFT gives reasonable results for these materials provided that the GGA is used [17]. For $\text{Mn}_5\text{Ge}_3\text{C}_{0.8}$ the DFT results suggest the presence of a 90° superexchange between Mn_{II} atoms and enhanced ferromagnetic Mn-Mn interactions mediated by carbon responsible for the strongly enhanced Curie temperature T_C compared to Mn_5Ge_3 [20]. Furthermore, it was shown that the interatomic distances can have a strong effect on the local magnetic moments and their interaction, in particular for the Mn moments [36]. Hence, it is essential to use valid lattice constants as input parameters for the DFT calculations to obtain reliable results for comparison with experimental data. In this work we used the lattice constants of films measured by x-ray diffraction [25]. Figures 1(b) and 1(c) show the lattice parameters a and c of the hexagonal structure for several samples. While the lattice shrinks with increasing carbon content x for $\text{Mn}_5\text{Ge}_3\text{C}_x$ it expands in the case of $\text{Mn}_5\text{Si}_3\text{C}_x$. Nonetheless, for both compounds the c/a ratio increases with x . This contrasting behavior between $\text{Mn}_5\text{Ge}_3\text{C}_x$ and $\text{Mn}_5\text{Si}_3\text{C}_x$ was reported earlier and demonstrates the different effect of carbon participating

TABLE I. Averaged local magnetic moment at the Mn_I and Mn_{II} sites of $Mn_5Ge_3C_x$ and $Mn_5Si_3C_x$, cf. Fig. 2(a). “calc” and “exp” indicate calculated and experimental values previously obtained by other groups.

Compound		Mn_5Ge_3	$Mn_5Ge_3C_{0.5}$	$Mn_5Ge_3C_{0.75}$	Mn_5Ge_3C	$Mn_5Si_3C_{0.5}$	$Mn_5Si_3C_{0.75}$	Mn_5Si_3C
m_I (μ_B/Mn_I)	This work	2.34	2.24	2.24	2.21	1.86	1.80	1.73
	calc	2.28 [19]			2.21 [20]			
	exp	1.96 [36]			2.20 [39]		2 [10]	
m_{II} (μ_B/Mn_{II})	This work	3.17	2.70	2.58	2.34	2.46	2.15	1.89
	calc	3.22 [19]			2.37 [20]			
	exp	3.23 [36]			2.20 [39]		2 [10]	

in the interatomic bonding [38]. Furthermore, the octahedral voids of the parent compounds are smaller in the case of Mn_5Si_3 than for Mn_5Ge_3 presumably prohibiting a further decrease of the Mn_5Si_3 lattice by incorporation of carbon.

The magnetic moments at the Mn_I and Mn_{II} sites obtained from the DFT calculations are shown in Table I. The averaged local magnetic moment of Mn in Mn_5Ge_3 is predicted to be 2.34 and 3.17 μ_B/Mn for Mn_I and Mn_{II} , which is close to the experimentally observed values of 1.96 and 3.23 μ_B/Mn and previously calculated values of 2.28 and 3.22 μ_B/Mn , respectively [19,36]. Reasonable agreement is also obtained for Mn_5Ge_3C and $Mn_5Si_3C_{0.75}$ by comparing with earlier work [10,20,39].

In both compounds, the incorporation of carbon into the hexagonal lattice gives rise to reduced Mn moments with increasing x and a lower magnetization presumably due to a hybridization between the carbon 2*p* and Mn 3*d* orbitals [20]. The Mn_{II} moments are more strongly affected by C due to their close vicinity to C compared to Mn_I . An NMR investigation performed on an epitaxially grown $Mn_5Ge_3C_{0.2}$ film proved that the Mn_{II} moment is reduced by 0.7 μ_B [35]. The calculated electronic DOS are shown in Fig. 2 for a collinear magnetic structure for various x . For each concentration x , the DOS integrated over all bands shows a dominating contribution from the electronic 3*d* band around ± 2 eV of

the Fermi level E_F corresponding to $E = 0$. Moreover, for both compounds the minority-spin band is always dominating over the majority-spin band and is stronger affected by the carbon incorporation, see Figs. 2(b) and 2(d). A clear difference between the two compounds is the larger separation of the *d* band peaks close to E_F for $Mn_5Ge_3C_x$ compared to $Mn_5Si_3C_x$. From the DOS at the Fermi level $N_\uparrow(0)$ and $N_\downarrow(0)$ of the spin-split bands we obtain the spin polarization $P_0 = (N_\uparrow - N_\downarrow)/(N_\uparrow + N_\downarrow)$.

B. Anisotropic magnetoresistance

Figure 3 shows the AMR ratio versus temperature T for both compounds, where data of samples with carbon

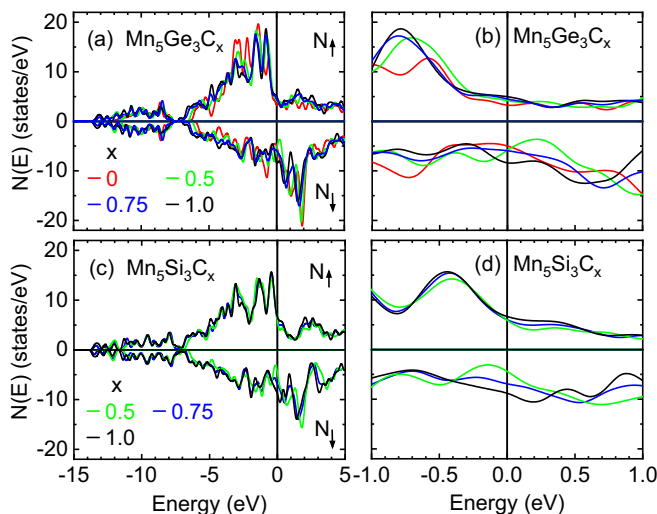


FIG. 2. (a), (b) Spin-split electronic DOS $N(E)$ of $Mn_5Ge_3C_x$. (c), (d) The same for $Mn_5Si_3C_x$. (b) and (d) show the details of the DOS around the Fermi level $E_F = 0$.

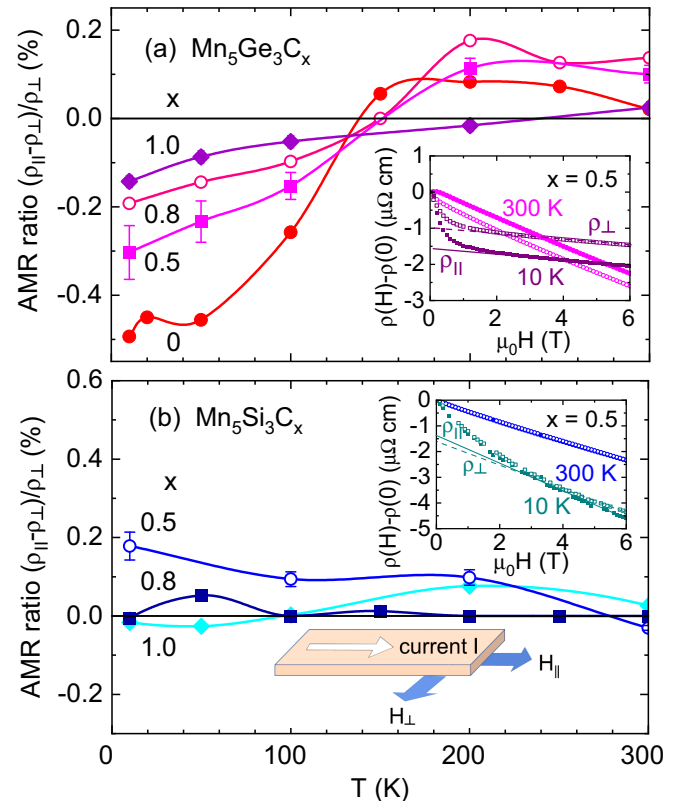


FIG. 3. Temperature dependence of the AMR ratio $\Delta\rho/\rho = (\rho_{\parallel} - \rho_{\perp})/\rho_{\perp}$ for (a) $Mn_5Ge_3C_x$ and (b) $Mn_5Si_3C_x$ films. Inset shows the resistivity in longitudinal and transverse orientation of the magnetic field H with respect to the current direction for $x = 0.5$ at 300 K and 10 K.

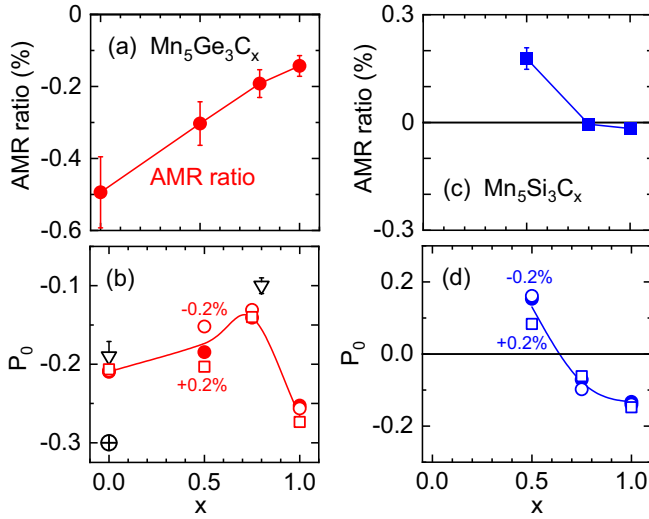


FIG. 4. Experimentally observed AMR ratio at $T = 10$ K and spin polarization $P_0 = (N_\uparrow - N_\downarrow)/(N_\uparrow + N_\downarrow)$ inferred from DFT calculations vs. carbon concentration x for (a), (b) $\text{Mn}_5\text{Ge}_3\text{C}_x$ and (c), (d) $\text{Mn}_5\text{Si}_3\text{C}_x$ (solid circles). Open circles (squares) indicate P_0 when assuming a lattice compression (expansion) of $-(+)$ 0.2%, see text for details. Previous DFT results for P_0 are also shown in (b): ∇ Ref. [20], \oplus Ref. [21].

concentrations $x = 0.5$ and 1 were added to data reported earlier [23]. The AMR ratio was determined from the measured resistivities $\rho_{\parallel}(H)$ and $\rho_{\perp}(H)$ in parallel and perpendicularly applied magnetic field H extrapolated from high magnetic fields well above saturation to $H = 0$, respectively, as shown in the insets of Fig. 3. By this procedure the AMR value is determined in magnetic saturation to minimize effects from domain reorientation or magnetic anisotropy.

The newly acquired data fit into the concentration dependence of the AMR ratio. For $\text{Mn}_5\text{Ge}_3\text{C}_x$, the AMR ratio is always negative at low temperatures and changes sign around 150 K while for $\text{Mn}_5\text{Si}_3\text{C}_x$ the AMR ratio is smaller and always positive. AMR ratio diminishes at high temperatures due to the increased spin-flip scattering by phonons and magnons. In the following we use the AMR ratio observed at $T = 10$ K for comparison with the DFT calculation.

IV. DISCUSSION

Figure 4 shows the measured AMR ratio at $T = 10$ K together with the spin polarization P_0 derived from DFT. For Mn_5Ge_3 and $\text{Mn}_5\text{Ge}_3\text{C}_{0.75}$ the obtained values are in good agreement with results obtained by first-principles calculations reported earlier [18–22].

However, for Mn_5Ge_3 the calculated negative values of P_0 are in contrast to a positive $P_0 = 0.15$ observed in spin-resolved photoemission spectroscopy [16]. This discrepancy was mentioned earlier and cannot be explained but the present work provides further evidence that the minority-spin subband is dominating the DOS as discussed in the following.

For both compounds we observe a clear correlation between the AMR ratio and P_0 which both increase or decrease with increasing x for $\text{Mn}_5\text{Ge}_3\text{C}_x$ [Fig. 4(a)] and $\text{Mn}_5\text{Si}_3\text{C}_x$ [Fig. 4(b)], respectively, except for $\text{Mn}_5\text{Ge}_3\text{C}_1$. In the latter,

$x = 1$ is beyond the concentration for which a maximum T_C was observed [4,9,34]. It is reasonable to assume that for $\text{Mn}_5\text{Ge}_3\text{C}_1$ the structure would be strongly compressed and carbon starts to introduce more disorder and generates local lattice distortions which give rise to a decreased $|P_0|$ and hence AMR ratio, in contrast to a larger $|P_0|$ obtained from DFT. This distortion of $\text{Mn}_5\text{Ge}_3\text{C}_1$ can be different for the calculated bulk compound and the prepared thin film. However, it is clearly seen that for $\text{Mn}_5\text{Ge}_3\text{C}_x$ the AMR ratio and P_0 are both negative for all x . The most prominent difference when compared to $\text{Mn}_5\text{Si}_3\text{C}_x$ is that for $\text{Mn}_5\text{Si}_3\text{C}_x$ both parameters are positive for $x = 0.5$ and both change sign between $x = 0.5$ and $x = 0.8$, cf. Fig. 4(b).

Since results from DFT are in general very sensitive to the crystallographic lattice parameters we additionally performed calculations for a compressed or expanded lattice, where we assumed a contraction of -0.2% or an expansion of $+0.2\%$ of each lattice constant. These results are also shown Figs. 4(b) and 4(d). The moderate variations in P_0 indicate that even for such large strains the overall behavior of $P_0(x)$ does not considerably change for both compounds. In particular, the sign change of $P_0(x)$ of $\text{Mn}_5\text{Si}_3\text{C}_x$ around between $x = 0.5$ and $x = 0.7$ remains.

For further analysis of the apparent correlation between AMR ratio and spin polarization we used the theoretical model developed by Kokada and Tsunoda who derived a general expression of the AMR ratio of ferromagnets by extension of the two-current model by Mott and Campbell and Fert [13,14]. They provide an intuitive explanation for the relation between the sign of the AMR ratio and the s - d scattering process. In this process, the resistance is dominated by scattering of delocalized conduction electrons expressed by $\rho_{s\uparrow(\downarrow)}$ into more localized $3d$ states expressed by $\rho_{s\rightarrow d\uparrow(\downarrow)}$ and negligible intraband scattering. Furthermore, it is considered that the final state of the scattering is the component of the current direction of distorted d orbitals which are oriented by the magnetization. In this model, the ratio $\rho_{s\rightarrow d\uparrow(\downarrow)}/\rho_{s\uparrow(\downarrow)}$ is treated as a variable parameter and spin-flip scattering is only due to disorder and/or magnons.

We use Eq. (42) of Ref. [13] and consider $\rho_{\uparrow\downarrow} = 0$ (no spin mixing) at low temperatures

$$\Delta\rho/\rho = \frac{\gamma(\rho_{s\rightarrow d\uparrow} - \rho_{s\rightarrow d\downarrow})(\rho_{s\uparrow} - \rho_{s\downarrow} + \rho_{s\rightarrow d\uparrow} - \rho_{s\rightarrow d\downarrow})}{(\rho_{s\uparrow} + \rho_{s\rightarrow d\uparrow})(\rho_{s\downarrow} + \rho_{s\rightarrow d\downarrow})}. \quad (1)$$

We note that the total DOS at E_F of both compounds is dominated by the $3d$ band contributing 91–92% and 93–94% to the total DOS of $\text{Mn}_5\text{Ge}_3\text{C}_x$ and $\text{Mn}_5\text{Si}_3\text{C}_x$, respectively. Furthermore, since the DOS of both spin subbands are not very different we make use of $\rho_{s\rightarrow d\uparrow}/\rho_{s\rightarrow d\downarrow} = N_\uparrow/N_\downarrow$ for a weak ferromagnet and obtain

$$\Delta\rho/\rho = 2\gamma\beta P_0 \left[\frac{1}{(\xi + \beta)(1 - P_0)} - \frac{1}{\beta(1 + P_0) + (1 - P_0)} \right], \quad (2)$$

where $\beta = \rho_{s\rightarrow d\downarrow}/\rho_{s\uparrow}$, $\xi = \rho_{s\downarrow}/\rho_{s\uparrow}$, and $\gamma = 0.01$ is the ratio between spin-orbit coupling and exchange energy [13,14].

Figure 5 shows calculated AMR ratios assuming $\rho_{s\rightarrow d\downarrow} < \rho_{s\uparrow}$. We find a qualitative agreement regarding the sign and absolute value of measured AMR ratios [Fig. 4] for

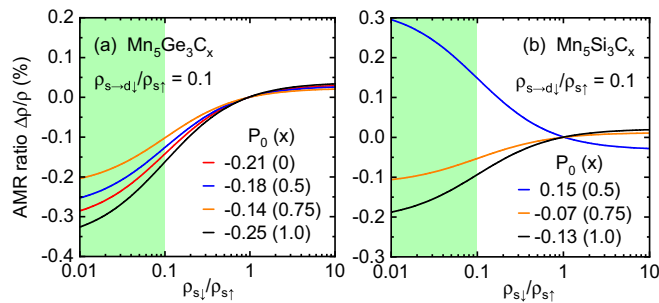


FIG. 5. AMR ratio at $T = 10$ K vs. $\xi = \rho_{s\downarrow}/\rho_{s\uparrow}$ calculated for $\rho_{s\rightarrow d\downarrow}/\rho_{s\uparrow} = 0.1$ and different values $P_0(x)$ for (a) $\text{Mn}_5\text{Ge}_3\text{C}_x$ and (b) $\text{Mn}_5\text{Si}_3\text{C}_x$ following Ref. [12], see text for details.

$\rho_{s\downarrow}/\rho_{s\uparrow} < 0.1$ indicated by the green area, i.e., for dominating minority-spin conduction in both compounds, $\rho_{s\downarrow} \ll \rho_{s\uparrow}$. This is even the case for $P_0 > 0$ as observed for $\text{Mn}_5\text{Si}_3\text{C}_{0.5}$ for which the sign change of the AMR is also reproduced for x between 0.5 and 0.75. It is important to mention that for $\rho_{s\rightarrow d\downarrow} > \rho_{s\uparrow}$ the model gives an AMR which is always

positive for all $\rho_{s\downarrow}/\rho_{s\uparrow}$ and is therefore not shown here. Furthermore, spin mixing has not been taken into account which would weaken the AMR as shown and would give rise to a diminished AMR ratio at elevated temperatures as mentioned above, see Fig. 3.

We conclude that our combined analysis of the experimentally measured AMR ratio and the spin-split electronic DOS obtained from DFT calculations give a consistent picture of the spin-dependent electronic transport in ferromagnetic $\text{Mn}_5\text{Ge}_3\text{C}_x$ and $\text{Mn}_5\text{Si}_3\text{C}_x$ films, providing strong evidence for a dominating minority spin-band conduction. This has to be taken into account for the implementation of these compounds as spin active electrodes in semiconductor spintronic devices and when considering current-induced magnetization switching phenomena [40].

ACKNOWLEDGMENTS

This work was supported by the Deutsche Forschungsgemeinschaft through Project No. SU225/3-1 and by the Chinese-German Mobilityprogramme Project No. M-0273.

- [1] I. Žutić, J. Fabian, and S. Das Sarma, *Rev. Mod. Phys.* **76**, 323 (2004).
- [2] R. Jansen, *Nat. Materials* **11**, 400 (2012).
- [3] C. Zeng, S. C. Erwin, L. C. Feldman, A. P. Li, R. Jin, Y. Song, J. R. Thompson, and H. H. Weitering, *Appl. Phys. Lett.* **83**, 5002 (2003).
- [4] V. L. Thanh, A. Spiesser, M.-T. Dau, S. F. Olive-Mendez, L. A. Michez, and M. Petit, *Adv. Nat. Sci. Nanosci. Nanotechnol.* **4**, 043002 (2013).
- [5] Y. Xie, Y. Yuan, M. Wang, C. Xu, R. Hübner, J. Grenzerl, Y.-J. Zeng, M. Helm, S. Zhou, and S. Prucnal, *Appl. Phys. Lett.* **113**, 222401 (2018).
- [6] J. Tang, C.-Y. Wang, L.-T. Chang, Y. Fan, T. Nie, M. Chan, W. Jiang, Y.-T. Chen, H.-J. Yang, H.-Y. Tuan, L.-J. Chen, and K. L. Wang, *Nano Lett.* **13**, 4036 (2013).
- [7] I. A. Fischer, L.-T. Chang, C. Sürgers, E. Rolseth, S. Reiter, S. Stefanov, S. Chiussi, J. Tang, K. L. Wang, and J. Schulze, *Appl. Phys. Lett.* **105**, 222408 (2014).
- [8] E. Voloshina and Y. Dedkov, *J. Phys. Chem. Lett.* **10**, 3212 (2019).
- [9] M. Gajdzik, C. Sürgers, M. T. Kelemen, and H. v. Löhneysen, *Journ. Magn. Magn. Mater.* **221**, 248 (2000).
- [10] M. Gajdzik, C. Sürgers, M. Kelemen, and H. v. Löhneysen, *J. Appl. Phys.* **87**, 6013 (2000).
- [11] T. R. McGuire and R. I. Potter, *IEEE Trans. Magn.* **11**, 1018 (1975).
- [12] M. Tsunoda, Y. Komazaki, S. Kokado, S. Isogami, C.-C. Chen, and M. Takahashi, *Appl. Phys. Express* **2**, 083001 (2009).
- [13] S. Kokado, M. Tsunoda, K. Harigaya, and A. Sakuma, *J. Phys. Soc. Jpn.* **81**, 024705 (2012).
- [14] S. Kokado and M. Tsunoda, *Adv. Mater. Res.* **750**, 978 (2013).
- [15] I. Mazin, *Phys. Rev. Lett.* **83**, 1427 (1999).
- [16] Y. S. Dedkov, M. Holder, G. Mayer, M. Fonin, and A. B. Preobrajenski, *J. Appl. Phys.* **105**, 073909 (2009).
- [17] E. Arras, D. Caliste, T. Deutsch, F. Lancon, and P. Pochet, *Phys. Rev. B* **83**, 174103 (2011).
- [18] R. P. Panguluri, C. Zeng, H. H. Weitering, J. M. Sullivan, S. C. Erwin, and B. Nadgorny, *Phys. Stat. Sol. (b)* **242**, R67 (2005).
- [19] S. Picozzi, A. Continenza, and A. J. Freeman, *Phys. Rev. B* **70**, 235205 (2004).
- [20] I. Slipukhina, E. Arras, P. Mavropoulos, and P. Pochet, *Appl. Phys. Lett.* **94**, 192505 (2009).
- [21] A. Stroppa, G. Kresse, and A. Continenza, *Appl. Phys. Lett.* **93**, 092502 (2008).
- [22] A. Stroppa and M. Peressi, *Phys. Stat. Sol. (a)* **204**, 44 (2007).
- [23] C. Sürgers, G. Fischer, P. Winkel, and H. v. Löhneysen, *Phys. Rev. B* **90**, 104421 (2014).
- [24] C.-E. Dutoit, V. O. Dolocan, M. Kuzmin, L. Michez, M. Petit, V. Le Thanh, B. Pigeau, and S. Bertaina, *J. Phys. D: Appl. Phys.* **49**, 045001 (2016).
- [25] R. Kraft, S. Srichandan, G. Fischer, and C. Sürgers, *J. Appl. Phys.* **128**, 033905 (2020).
- [26] P. E. Blöchl, *Phys. Rev. B* **50**, 17953 (1994).
- [27] G. Kresse and D. Joubert, *Phys. Rev. B* **59**, 1758 (1999).
- [28] G. Kresse and J. Hafner, *Phys. Rev. B* **47**, 558(R) (1993).
- [29] G. Kresse and J. Hafner, *Phys. Rev. B* **49**, 14251 (1994).
- [30] G. Kresse and J. Furthmüller, *Comput. Mat. Sci.* **6**, 15 (1996).
- [31] G. Kresse and J. Furthmüller, *Phys. Rev. B* **54**, 11169 (1996).
- [32] J. P. Perdew, K. Burke, and M. Ernzerhof, *Phys. Rev. Lett.* **77**, 3865 (1996).
- [33] R. Elmer, M. Berg, L. Carlen, B. Jakobsson, B. Noren, A. Oskarsson, G. Ericsson, J. Julien, T.F. Thorsteinsen, M. Guttormsen, G. Lovhoiden, V. Bellini, E. Grosse, C. Muntz, P. Senger, and L. Westerberg, *Phys. Rev. Lett.* **78**, 1396 (1997).
- [34] A. Spiesser, I. Slipukhina, M.-T. Dau, E. Arras, V. Le Thanh, L. Michez, P. Pochet, H. Saito, S. Yuasa, M. Jamet, and J. Derrien, *Phys. Rev. B* **84**, 165203 (2011).
- [35] R. Kalvig, E. Jedryka, M. Wojcik, M. Petit, and L. Michez, *Phys. Rev. B* **101**, 094401 (2020).

- [36] J. B. Forsyth and P. J. Brown, *J. Phys. Condens. Matter* **2**, 2713 (1990).
- [37] K. Momma and F. Izumi, *J. Appl. Crystallogr.* **44**, 1272 (2011).
- [38] C. Sürgers, K. Potzger, and G. Fischer, *J. Chem. Sci.* **121**, 173 (2009).
- [39] C. Sürgers, K. Potzger, T. Strache, W. Möller, G. Fischer, N. Joshi, and H. v. Löhneysen, *Appl. Phys. Lett.* **93**, 062503 (2008).
- [40] M. AlHajDarwish, H. Kurt, S. Urazhdin, A. Fert, R. Loloee, W. P. Pratt, Jr., and J. Bass, *Phys. Rev. Lett.* **93**, 157203 (2004).